INSTITUTE OF PHYSICS PUBLISHING PLASMA SOURCES SCIENCE AND TECHNOLOGY

Plasma Sources Sci. Technol. **15** (2006) 8–17 doi:10.1088/0963-0252/15/1/002

Comparative study of diffuse barrier discharges in neon and helium

Z Navrátil[1,2], R Brandenburg[3,4], D Trunec[1], A Brablec[1], P St'ahel[1], H-E Wagner[3] and Z Kopecký[5]

[1] Department of Physical Electronics, Faculty of Science, Masaryk University in Brno, Kotlářská 2, CZ-611 37 Brno, Czech Republic
[2] Department of General Physics, Faculty of Science, Masaryk University in Brno, Kotlářská 2, CZ-611 37 Brno, Czech Republic
[3] Institute of Physics, Ernst-Moritz-Arndt University of Greifswald, Domstrasse 10a, D-17489 Greifswald, Germany
[4] Institute of Low Temperature Plasma Physics, F.-L.-Jahn-Strasse 19, D-17489 Greifswald, Germany
[5] Department of Theoretical Physics and Astrophysics, Faculty of Science, Masaryk University in Brno, Kotlářská 2, CZ-611 37 Brno, Czech Republic

E-mail: zdenek@physics.muni.cz

Received 10 February 2005
Published 18 November 2005
Online at stacks.iop.org/PSST/15/8

Abstract

Diffuse dielectric barrier discharges in neon and helium at atmospheric pressure were studied. The discharges were generated between two metal electrodes, both covered by an alumina layer and driven by ac voltage of frequency 10 kHz. The discharge gap was 2.2 mm and 5 mm, respectively.

The discharges were investigated by electrical measurements and by temporally and spatially resolved optical emission spectroscopy. The experimental results revealed similar discharge behaviour in both gases being considered. Although the discharges were ignited at slightly different electric field strengths, their evolutions were found to be similar. At maximum discharge current the spatial light intensity distribution was characterized by the formation of a cathode fall. A difference was observed in the magnitudes of the current density only.

In addition to the regime with a single discharge pulse per voltage half period $T/2$, a discharge mode with two and more subsequent current pulses per $T/2$ (also referred to as the pseudoglow discharge regime in the literature) was obtained due to an increase in the voltage amplitude or an admixture of nitrogen.

(Some figures in this article are in colour only in the electronic version)

1. Introduction

Dielectric barrier discharges (DBDs) are convenient plasma sources for the generation of non-thermal plasmas at atmospheric pressure. Usually the DBD plasma consists of many tiny microdischarges (or filaments) of nanosecond or microsecond duration. The properties of these so-called filamentary discharges and the actual microdischarges have been studied elsewhere (see e.g. Eliasson and Kogelschatz(1991), Gibalov and Pietsch(2000), Kozlov *et al* (2001)).

Under special operation conditions, particularly in certain gases or gas mixtures, so-called diffuse DBDs can be obtained in a DBD configuration. These discharges are also referred to as homogeneous DBDs or atmospheric pressure glow discharges (APGDs). So far, diffuse DBD has been revealed and investigated in helium, neon, nitrogen and argon with admixtures of acetone (see e.g. Massines *et al* (1998), Gherardi *et al* (2000), Trunec *et al* (2001)). The homogeneity of the diffuse DBD is very desirable for industrial applications, especially for surface treatment processes.

Diffuse discharges in helium, at conditions similar to those being considered in this paper, have been studied by means of electrical measurements and short time exposure photography (e.g. Massines *et al* (1998), Radu *et al* (2004)), by temporally resolved optical emission spectroscopy(Ricard *et al* 1999) and by numerical modelling (e.g.Golubovskii *et al* (2003)). It was found that the diffuse DBD in helium is a transient glow discharge, since the formation of a cathode fall and a positive column were observed. According to Massines *et al* (1998) electrons and ions are trapped in the positive column from one discharge cycle to the following one. This process leads to a pre-ionization of the gas below the ignition voltage and is manifested in the so-called 'residual current peak', a small increase of the discharge current about 2 μs after the inversion of the voltage polarity. Furthermore Massines *et al* (1998) as well as Müller and Zahn(1996), Golubovskii *et al* (2003) and Radu *et al* (2004) pointed out the important role of indirect ionization processes, e.g. Penning ionization of N_2 molecules originating from dilute gas impurities by helium metastable states.

Trunec *et al* (2001) demonstrated that a diffuse DBD can be generated in neon as well. But the character of the discharge remains unknown at this point of time. As demonstrated by different teams (e.g. Gherardi *et al* (2000), Kozlov *et al* (2005)) in nitrogen a different kind of diffuse DBD is generated. This discharge reveals the structure of a Townsend discharge. No significant space charges are formed; the maximum of excited species was found in front of the anode.

The distinction between the diffuse and filamentary regimes is mostly monitored with the use of electrical measurements. However, the distinction between the different discharge structures (as concerning Townsend or glow discharge) and the study of a discharge development can be performed by means of optical methods with a temporal and spatial resolution as short time exposure photography or temporally and spatially resolved optical emission spectroscopy.

In this work spatially and spectrally resolved time-correlated single photon counting (TC-SPC) was used for the comparative study of the diffuse DBDs in neon and helium. A description of our experimental set-up is given in section 2. The results are presented in section 3. While section 3.1 is concerned with the electrical measurements, in section 3.2 overview spectra and the spatio-temporally resolved discharge development are discussed.

2. Experimental set-up

The experimental set-up is schematically shown in figure 1. It is basically the same set-up as described by Kozlov *et al* (2001) and Kozlov *et al* (2005), and it was originally equipped for cross-correlation spectroscopy (CCS) on DBD-microdischarges. The discharge was generated in a parallel plane discharge cell consisting of two metal electrodes (1) both covered by a 0.7 mm thick alumina (Al_2O_3) layer (2) with a relative permittivity of $\epsilon_r = 9.4 \pm 0.3$. The electrode area was 20 mm × 20 mm and the area of the covering dielectric plates was 30 mm × 36 mm. The electrodes were fixed by two space holders made of organic glass (3) ensuring a constant discharge gap. Two discharge cells, with discharge gaps of 2.2 mm and 5.0 mm respectively, were used.

The discharge cell was placed in a stainless steel vacuum chamber connected to a rotary vacuum pump (ILMVAC PK 4D rotary pump) and to a gas supply, with a flow control unit. The chamber was evacuated down to 10 Pa first and then filled with neon or helium gas (purity 99.999 vol%) slightly above atmospheric pressure. After that, the gas outlet was opened to the atmosphere, sustaining the discharge in the gas flowing regime. Using a sealing ring with a nozzle on the gas entrance and a pipe (4) the gas was directly injected into the discharge volume. A small admixture of a second gas (e.g. nitrogen) could be added to the working gas. The pressure in the chamber was controlled by ILMVAC Piza 2000 manometer. The total gas flow rate was 450 sccm, kept by MKS 1259 CC gas flow controllers.

The discharge was driven by an ac voltage of frequency 10 kHz. The sinusoidal voltage signal from a Voltcraft MXG-9802 function generator was amplified using a Conrad Skyline-Storm amplifier (400 W) and transformed to a high voltage signal with amplitude $U_{a0} = 0.5$–2 kV. The applied voltage U_a and the discharge current I were measured by Tektronics TDS 380 (400 MHz bandwidth, 2 GSamples/s) digital oscilloscope. The applied voltage U_a was measured via a 1000 : 1 voltage divider; the current I was monitored by measuring the voltage across a 100 Ω resistor, connected in series with the discharge cell. The gap voltage U_g and the memory voltage U_m were calculated from the applied voltage U_a and the current I using equations (1) and (2) as described by Massines *et al* (1998):

$$U_a(t) = U_g(t) + U_m(t), \tag{1}$$

$$U_m(t) = U_m(t_0) + \frac{1}{C_d}\int_{t_0}^{t} I(t')\,dt', \tag{2}$$

where $C_d \approx 24$ pF is the dielectric capacitance of the dielectric barriers, and $U_m(t_0)$ is the initial memory voltage across the dielectrics, which was adjusted in order to obtain the symmetrical evolution of the gap voltage (i.e. $\langle U_g \rangle = 0$).

The chamber was equipped with two quartz windows for discharge diagnostics. The window (5) served for direct observations, the other (6) was used for spatially and temporally resolved optical emission spectroscopy measurements. The lens (7) was placed at a distance of double focal length $2f_L$ from the discharge cell centre, imaging the discharge $1:(-1)$ onto an optical slit (8). This optical slit, 0.3 mm wide, was moved in the image and collected the light from a narrow discharge area, providing a one-dimensional spatial resolution along the discharge gap. Thus the slit was placed together with a lens (9) and the end of an optical fibre on an optical table, which was vertically adjustable by a computer controlled stepper motor. The lens (9) was used to project the slit onto the fibre entrance.

The optical fibre led to a Jobin Yvon TRIAX 320 spectrometer. The overview spectra were taken with a standard R 928 Hamamatsu photomultiplier (not shown in figure 1). For temporally resolved measurements the light was detected by water cooled highly sensitive PMH-100-4 photomultiplier (Hamamatsu) and analysed by means of TC-SPC module (SPC-530, Becker and Hickl). The SPC module was originally

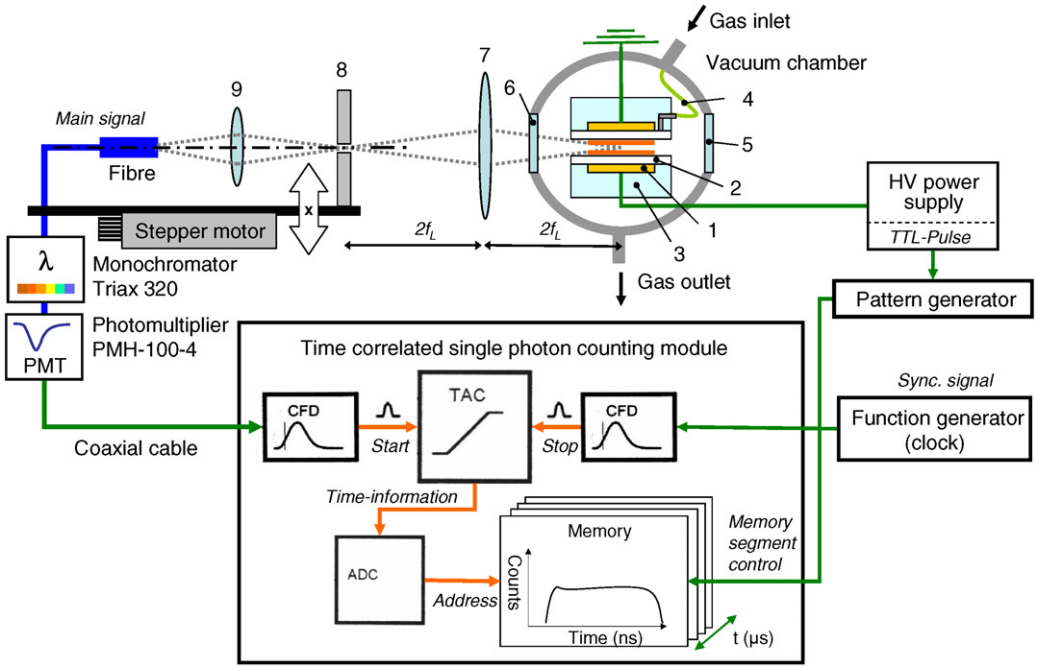

Figure 1. Scheme of the experimental set-up. (1) Metal electrode, (2) dielectric layer, (3) block of organic glass, (4) pipe, (5) and (6) quartz windows, (7) and (9) quartz lenses and (8) slit.

designed for the CCS method, and it had to be modified to investigate the diffuse DBD (Kozlov *et al* 2005). The diffuse DBDs produce periodical light pulses with a duration of typically several microseconds. Since the CCS apparatus was designed for optical triggering using statistically occurring light pulses with a duration in the nanosecond-range, the synchronization signal was missing. Therefore, an external independent function generator was used to provide the synchronization signal. The time-resolution of the photon counting procedure was realized by the pattern generator, which controlled the memory segment allocation of the SPC device. Since the discharge was periodical, the pattern generator was triggered directly by the power supply. A maximum time-resolution of 0.4 μs could be achieved with the apparatus.

3. Results and discussion

3.1. Electrical characteristics

Typical current and voltage oscillograms of diffuse DBDs burning in 5 mm discharge cell in pure neon and helium are shown in figure 2. The applied voltage was sinusoidal in both cases, except the voltage drop during the current pulse. This voltage drop was due to the limitations of the power supply. The breakdown voltage was evidently different with regard to both neon and helium. Before the current peak starts to rise, the applied voltage reached values of 0.3 kV and 0.7 kV in neon and helium, respectively. The gap voltage thus reached values of 0.7 kV and 1.3 kV in neon and helium, respectively. This difference is to be expected when comparing the energy dependences of neon and helium ionization cross sections (see figure 3). The ionization cross section of neon has a lower threshold energy than that of helium, and it is also higher above the threshold. Thus at comparable low electric field strength the ionization rate in neon can be expected to be higher than that of helium.

If the value of the applied voltage is close to the breakdown voltage, a single current peak per voltage half period is observed; the discharge operates in the so-called single peak mode (SPM). When comparing figures the current peaks of neon and helium discharge appear very similar. First a fast current increase (lasting about 4 μs) is observed in both cases, followed by a decay of about 20 μs. This current discharges and charges the dielectrics (see the slope of the memory voltage). The change of the memory voltage and the drop of the applied voltage (due to the limitations of the power supply) results in the drop of the gap voltage and the current decrease.

As observed by Mangolini *et al* (2002) as well as by Radu *et al* (2003), a higher applied voltage or a small admixture of nitrogen in the range of 100–800 ppm produced additional current peaks within the same half period. Up to four current peaks per $T/2$ could be investigated using our set-up. The electrical characteristics of this so-called double peak mode (DPM), also referred to as pseudoglow discharge regime and first reported by Bartnikas(1968) (see Radu *et al* (2003)), are displayed in figure 4. When the current decays at the end of the preceding peak, the applied and the gap voltage increase again, and a second breakdown can take place.

If nitrogen is admixed, electrons and N_2^+ ions are created by Penning effect (equations (3) and (4) and similarly for helium), which is the dominating ionization process in the time of current pulse decay (Radu *et al* 2003, Mangolini *et al* 2004):

$$\mathrm{Ne}(3s'[1/2]_0, 3s[3/2]_2) + \mathrm{N_2} \rightarrow \mathrm{N_2^+} + \mathrm{Ne} + \mathrm{e^-}, \quad (3)$$

$$\mathrm{Ne_2^*} + \mathrm{N_2} \rightarrow \mathrm{N_2^+} + 2\mathrm{Ne} + \mathrm{e^-}. \quad (4)$$

The generation of free electrons by this additional process results in a decrease of the voltage required for the breakdown.

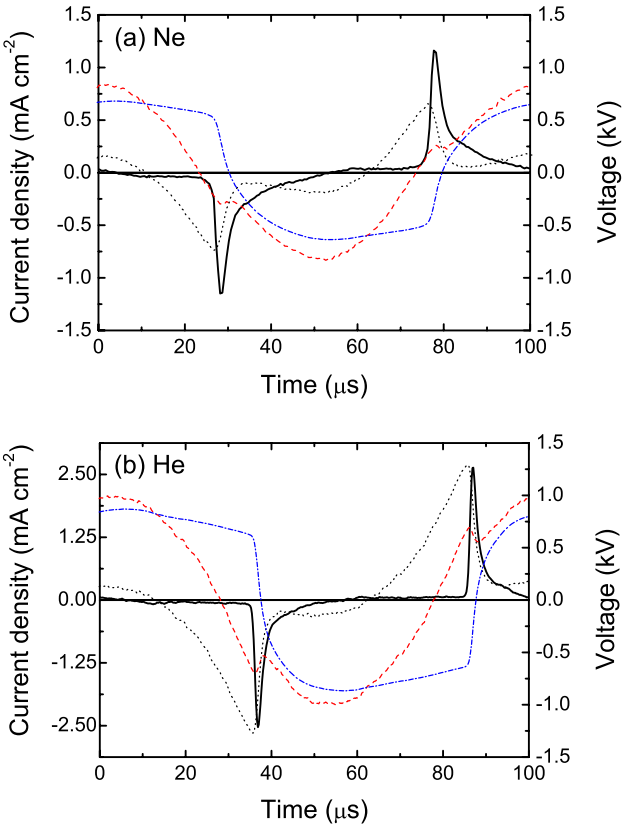

Figure 2. The current (——), applied voltage (- - - -), gap voltage (· · · · · ·) and memory voltage (— · —) evolution of the diffuse discharge in neon (*a*) and helium (*b*) in SPM.

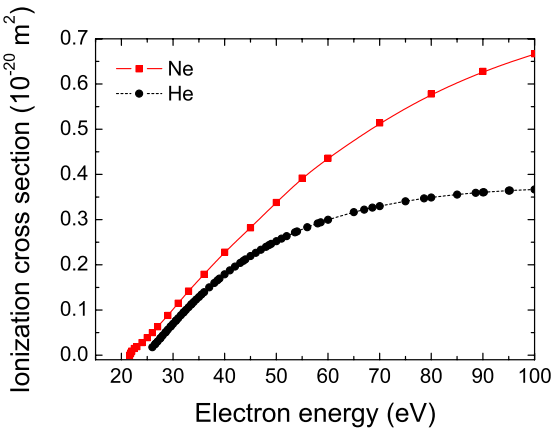

Figure 3. Total ionization cross sections of neon (Wetzel *et al* 1987) and helium (Kim and Rudd1994). The ionization energy is 21.6 eV and 24.6 eV, respectively.

Consequently, the second discharge is ignited at lower gap voltage than at the first breakdown (see figure 4). This explanation is in agreement with the discussion of Radu *et al* (2003) as well as of Mangolini *et al* (2002). The former discussed in great detail the influence of impurities, voltage amplitude and frequency in discharge cells with a gap of 0.5 mm.

In figure 5 an enlarged view of the current oscillogram is shown. A small 'residual current peak' was registered in our

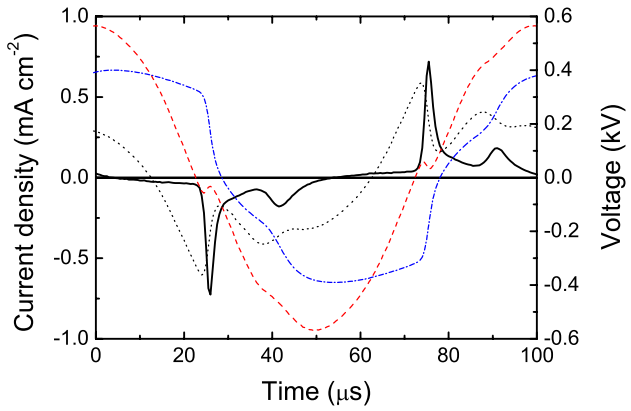

Figure 4. The current (——), applied voltage (- - - -), gap voltage (· · · · · ·) and memory voltage (— · —) evolution of the diffuse neon discharge in DPM.

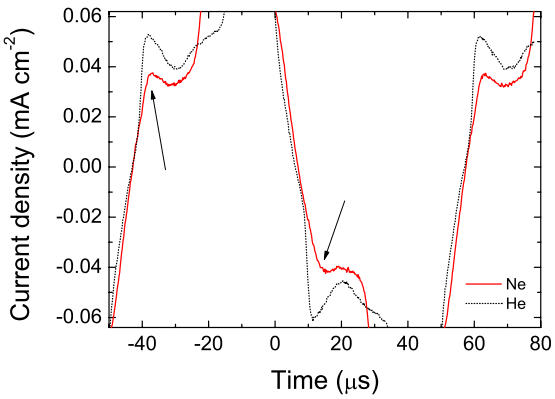

Figure 5. Enlarged view of the current oscillograms, showing the 'residual current peak' in diffuse DBDs in neon and helium. The helium current oscillogram is shifted in time for better comparison.

experiments in neon and helium with a similar magnitude as described by Massines *et al* (1998) (see the arrows in figure 5). However, the high luminosity of neon lines allowed us to assign the occurrence of such a current peak to a small spurious discharge burning on the edge of the dielectric layer, which appeared only at a narrow band of voltage frequencies approximately at 10 kHz. Furthermore, in the discharge cell with a gap of 2.2 mm a diffuse DBD was generated, but no residual current peak was observed. From our results, we suggest that free electrons from the previous discharge cannot remain in the area of the positive column of the transient glow discharge. Furthermore, we consider the indirect ionization involving long-lived species such as metastables and excimers to be fundamental for the generation of a diffuse DBD in helium and neon. Similarly Mangolini *et al* (2004) modelling the helium diffuse discharge came to the conclusion that most electrons leave the discharge gap after the current pulse, and up to the formation of the next breakdown the Penning ionization of nitrogen is by far the dominant source of electrons.

3.2. Optical emission spectroscopy

3.2.1. Overview spectra. Overview spectra of the light emitted by the SPM discharge in pure neon and helium are shown in figures 6(*a*) and (*b*), respectively. In both cases

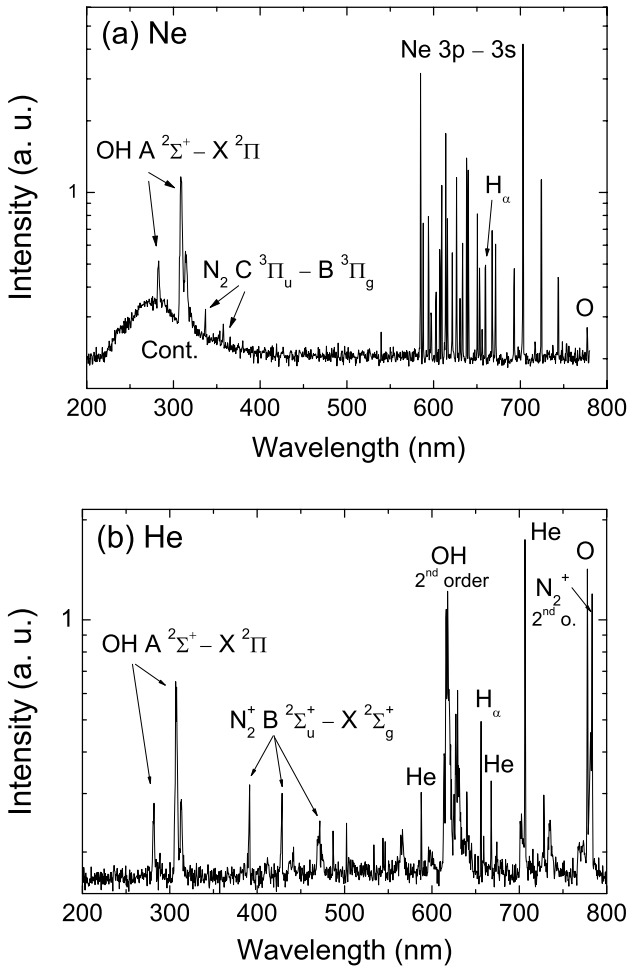

Figure 6. The typical overview spectra of diffuse DBDs in SPM (*a*) in neon and (*b*) in helium.

the spectra consisted of atomic lines of the working gas (neon, helium) as well as of atomic lines and molecular bands originating from inevitable gas impurities (nitrogen, hydrogen, oxygen and hydroxyl-radical). The impurities can be present in the working gas as well as be desorbed from the chamber walls and the dielectrics. In the case of neon, the atomic spectral lines of the transitions between the states $2p^5\,3p \rightarrow 2p^5\,3s$ of neon ($2p_i \rightarrow 1s_j$ in Paschen notation) were the most intensive. Although our diagnostic tool was optimized for the measurements in the near UV-region, no lines in the range 335–370 nm, originating from $2p^5\,4p$ states, were registered. Since some cross sections for electron impact excitation from the ground state to the levels $2p^5\,3p$ ($E_{\rm exc} \approx 18.7$ eV) and $2p^5\,4p$ ($E_{\rm exc} \approx 20.3$ eV) are similar above the threshold (Meneses *et al* 2002), a strong decay of the electron energy distribution function to higher energies is indicated by our experimental findings. Apart from neon lines, hydrogen atomic lines H_α and H_β at 656.3 nm and 486.1 nm, respectively, oxygen triplet line at 777 nm ($3p\,^5P \rightarrow 3s\,^5S^\circ$), N_2 second positive system ($C\,^3\Pi_u \rightarrow B\,^3\Pi_g$) and OH molecular system ($A\,^2\Sigma^+ \rightarrow X\,^2\Pi$) were observed. When the amount of the impurities was low (i.e. nitrogen bands were weak), a continuum in the wavelength range 220–450 nm was registered. The origin of this continuum is unclear, but its shape is quite similar to bremsstrahlung continuum of electrons impacting on neutral atoms observed by Lissovski and Treshchalov(2003) and Rutscher and Pfau(1976). However, numerical simulations with the corresponding plasma parameters (not presented here) and the time development of the continuum did not validate this explanation (see the discussion in section 3.2.3). According to Bojčenko *et al* (1993), a very similar continuum is produced by radiative transitions out of highly excited Rydberg Ne_2 molecules, or by transition between states correlating with Ne^{+*}+Ne and Ne^++Ne^*. To clarify the origin of this continuum further investigation is needed.

In the case of helium, several helium lines were intensive: at 706.5 nm ($3s\,^3S_1 \rightarrow 2p\,^3P$), 587.6 nm ($3d\,^3D \rightarrow 2p\,^3P$) and 667.8 nm ($3d\,^1D_2 \rightarrow 2p\,^1P_1$). As in neon the lines of oxygen and hydrogen as well as OH bands were present, but the N_2^+ first negative system ($B\,^2\Sigma_u^+ \rightarrow X\,^2\Sigma_g^+$) was the dominant nitrogen system due to the effective Penning ionization of nitrogen molecules by helium metastables. Comparable to the results in neon, when the degree of gas impurity was low, a weak continuum was observed in the range 250–800 nm (not seen in the figure).

3.2.2. Temporally resolved spectra. The intensive lines and bands in the overview spectra were further investigated by means of temporally and spatially resolved optical emission spectroscopy. The temporal intensity development of investigated lines was always measured at 24 positions along the whole discharge gap. These spatio-temporally resolved data are presented in section 3.2.3. In order to obtain the temporal intensity development only, the individual temporal intensity evolutions measured at different positions have been summarized. The intensities were normalized to their maximum values in order to compare the temporal dependences of various spectral lines. The results of this procedure are displayed in figure 7.

The temporally resolved intensity development of the spectral lines can be used to estimate the excitation mechanism of radiative states (in comparison with the temporal development of the discharge current). Whereas the direct excitation by energetic electrons occurs primarily at high electric field and electron concentration during the current pulse, indirect excitation processes involving e.g. metastables (excitation transfer, Penning ionization, recombination etc) will excite species even after the current pulse. In the case of neon (figure 7(*a*)), the temporally resolved intensities of two different lines originating from different upper states are shown. Their development is approximately the same and promptly follows the current first, but their decay is even faster (in comparison with the current). Therefore their upper states must be primarily populated by electron impact. The intensity evolution of the N_2 second positive system shows the best agreement with the current pulse. Initially it quickly reaches the maximum as the neon lines, but it decreases comparatively slowly. However, the slower decrease can be caused by the increase of the intensity of continuum (compare these two curves), which forms the background for the nitrogen system. Therefore the temporal evolution of nitrogen emission can also have a sharp maximum, and it can be excited mainly by electron impact as well. Oxygen and hydrogen and OH emissions are

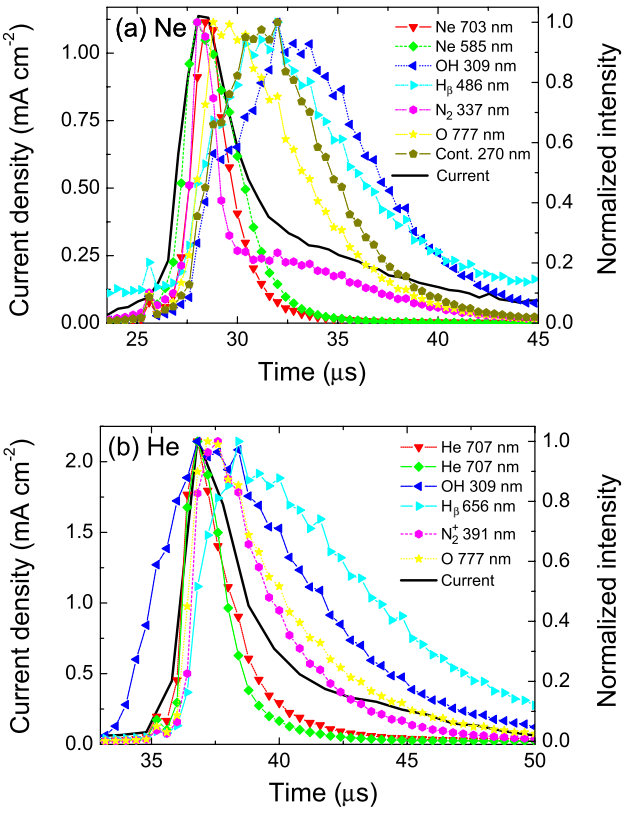

Figure 7. The temporal intensity development of various emissions of (*a*) neon discharge and (*b*) helium discharge in comparison with the discharge current (——).

clearly delayed in respect of the current pulse. This is due to the necessary preceding dissociation and ionization of the impurity species and due to the participation of metastables in these processes. The excitation mechanism of OH, which is the most delayed emission, is further discussed in section 3.2.3. The delay of the continuum intensity maximum probably excludes the possibility of being a bremsstrahlung radiation on neutrals, since electrons with energy of several electronvolts are needed in such a process (which are not expected to be present in the discharge after the current pulse).

In the case of helium (figure 7(*b*)), the same helium line at 707 nm was measured twice, at the beginning as the first measured line and then later after the measurement of other emissions (N_2^+, OH and H), in order to test the discharge stability and the reproducibility of the presented results. As can be seen in the figure, these two temporal dependences differ only slightly, and their maxima are as sharp as those of the neon lines. Consequently, helium is excited by the electron impact. The intensity dependences of impurity emissions denote the role of metastables as in the case of the neon discharge. Quite peculiar is the development of OH, the intensity of which increases faster than the discharge current.

3.2.3. Temporally and spatially resolved spectra. The temporally and spatially resolved intensity distributions of 5 mm SPM diffuse discharge in neon and helium are displayed in figures 8 and 9, respectively. These figures show the normalized intensity of various lines and bands in a logarithmic scale within almost the whole voltage period ($T = 100\,\mu$s) and resolved along the discharge gap. In the case of neon, the intensity distributions of the neon line at 703.2 nm, the N_2 second positive system at 337.1 nm, OH system at 309.0 nm, continuum at 270.0 nm, H_β at 486.1 nm and O triplet line at 777 nm are shown (figure 8). Wavelength 270 nm, at which the continuum was measured, was chosen in order to avoid an overlapping of the intensity of the OH system. In the case of helium, the intensity distributions of the helium line at 706.5 nm, N_2^+ first negative system at 391.4 nm, OH system at 309.0 nm and H_α at 656.3 nm are shown (figure 9).

The common discharge characteristic is that two intensity maxima appear within one voltage period. They can be clearly assigned to the two current pulses in the period, as they occur approximately at the same time (with an eventual small shift depending on the radiating specie). Since the voltage commutes between the current peaks, the positions of the electrodes exchange in the figures. In all figures, which display the whole period, the cathode is at the bottom of the figure first and the anode at the top (for $t < 62\,\mu$s), and vice versa. As the magnitudes of the positive and negative current peaks were nearly the same, the electrode system was symmetrical, and the optical system was carefully adjusted; no substantial difference was registered between both polarities—the intensity maxima appear similarly as mirrored by the plane passing through the gap centre.

The intensity distributions of neon and helium lines appear to be very similar. In both figures a cathode directed wave of increasing luminosity starts in the middle of the discharge gap and propagates to the cathode within 2 μs. Roughly 2.5 μs after its arrival at the cathode a second maximum of emission is registered at the anode, but with lower intensity than at the cathode. This result resembles the structure of a dc glow discharge with an intensive cathode light and a less intensive positive column. A small area of lower intensity, located between the cathode light and the positive column, which can be clearly seen in particular in neon (and in the case of the oxygen line of the neon discharge, too), evokes the Faraday dark space. The intensity is not zero, probably due to reflections. Cathode glow and negative glow cannot be resolved, since these regions are very close to each other at atmospheric pressure (Raizer1991, Massines *et al* 1998). The observed development is in agreement with the Townsend mechanism of the discharge breakdown, which presumes the discharge sustenance by secondary electrons being created by ion bombardment of the cathode and by photoionization. These findings are also in agreement with observations and numerical modelling carried out by Massines *et al* (1998) and Golubovskii *et al* (2003). In particular, the diagram of ionization rate in the breakdown phase in Golubovskii *et al* (2003) (see figure 8 of this reference) is very similar to the measured intensity distribution, although it was calculated for slightly different parameters.

The narrow (i.e. short in time) intensity maxima of both neon and helium line reflect the direct excitation of the atoms by electron collisions. The most important difference between the evolution of the neon and helium lines is the time of intensity onset as the breakdown in helium occurs later at a higher electric field.

The intensity maxima of most of the impurities (OH, O, H) are broader and shifted in time. This is due to the necessary

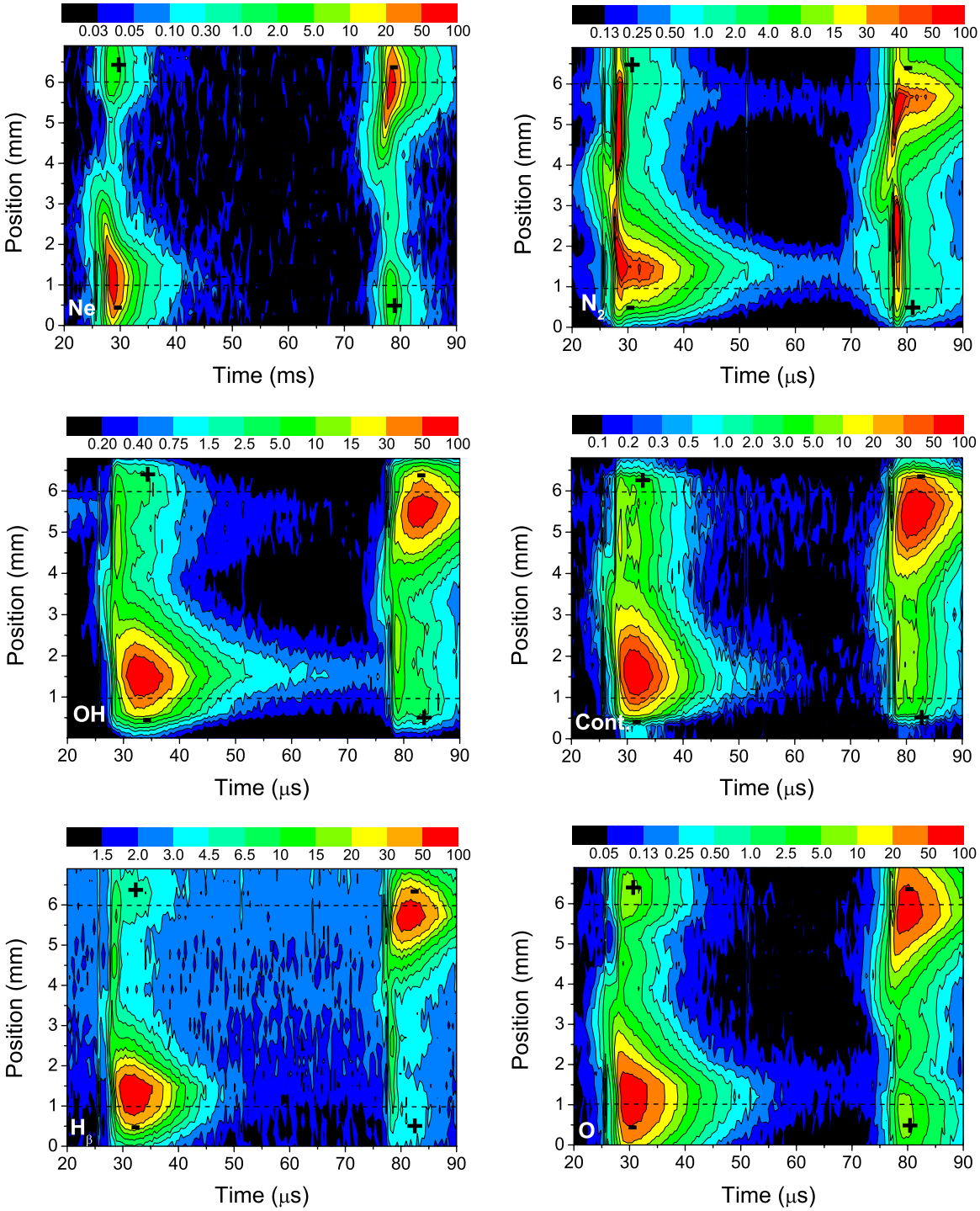

Figure 8. Spatially and temporally resolved intensity distributions of neon SPM diffuse discharge in a 5 mm cell. The relative intensity of the neon line at 703.2 nm, the N_2 second positive system at 337.1 nm, OH system at 309.0 nm, continuum at 270.0 nm, H_β at 486.1 nm and O triplet line at 777 nm are plotted in a logarithmic scale versus the time and the position across the discharge gap. The cathode is located at the bottom first, then at the top. The positions of the electrodes (i.e. of the dielectric layers) are marked out by the dashed lines.

dissociation and ionization of the impurities to form H and OH radicals and due to the participation of metastables in these processes. However, the intensity distribution of the light emitted by impurities basically follows the structure of the neon or helium line with intensive cathode directed light and less intensive anode light. The only exception is the emission of the N_2 second positive system of the neon discharge. Here the maximum value of the anode light intensity is comparable to that at the cathode and further persists (together with the emission at the cathode) throughout the whole period. The strong intensity maximum near the anode resembles the intensity development of the space charge free Townsend discharge in pure nitrogen (Brandenburg *et al* 2002). This similarity is moreover increased by the fact that the displayed

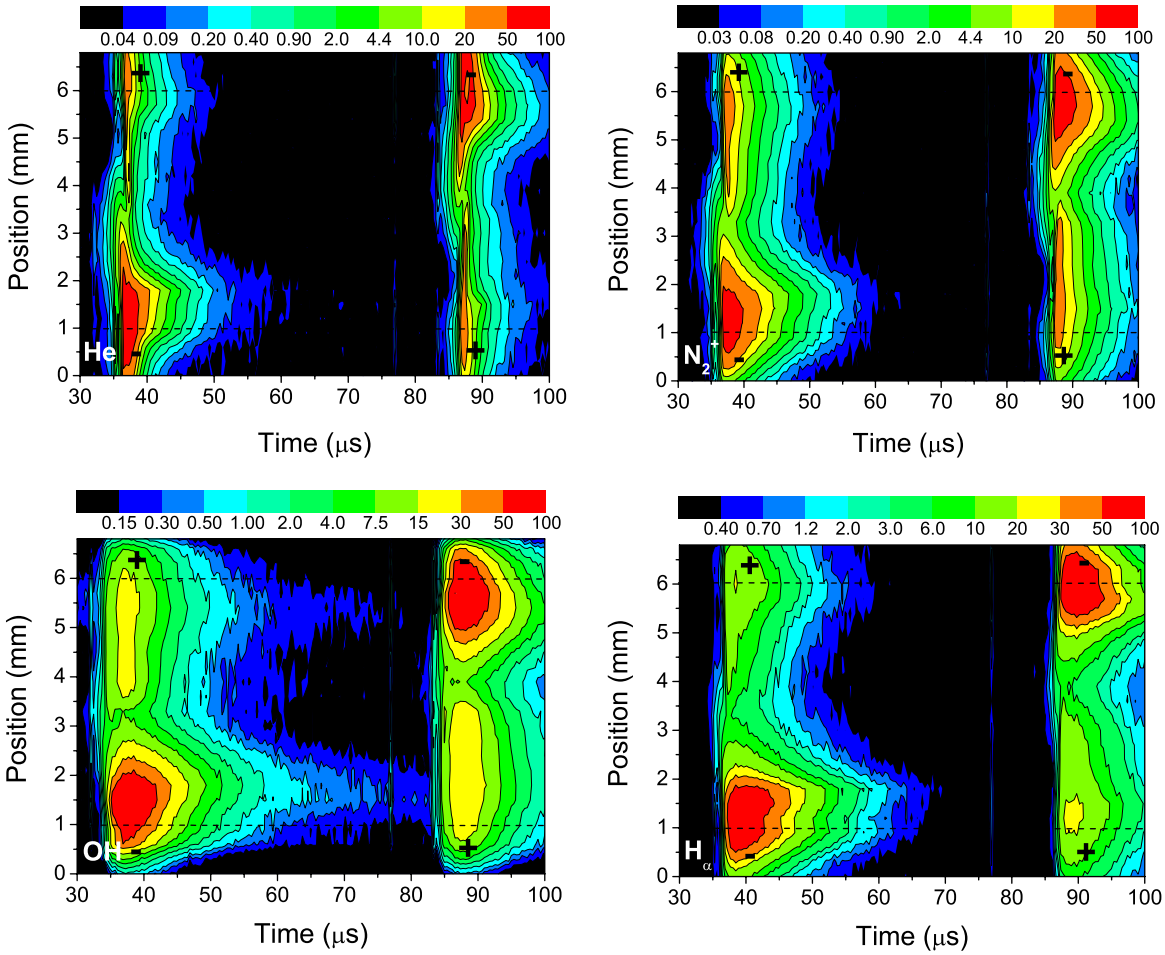

Figure 9. Spatially and temporally resolved intensity distributions of helium SPM diffuse discharge in a 5 mm cell. The relative intensity of helium line at 706.5 nm, N_2^+ first negative system at 391.4 nm, OH system at 309.0 nm and H_α at 656.3 nm are plotted in a logarithmic scale versus the time and the position across the discharge gap. The cathode is located at the bottom first, then at the top. The positions of the electrodes are marked out by the dashed lines.

intensity of N_2 partially belongs to the continuum, being—especially in the area of the cathode maximum—a relatively intensive background.

Besides N_2 emission of the second positive system, OH emission is observed throughout the voltage period in both neon and helium discharges. This is again in close agreement with Massines *et al* (1998), where the whole period of lasting light emission of helium diffuse discharge operating at similar conditions was reported. The radiation of OH in the afterglow (9) is explained in helium (Ricard *et al* 1999) considering the production of radiative states OH(A) by the recombination of H_2O^+ ions—reaction (8), which are created by metastable helium atoms in reactions as in (5) or by metastable helium dimers $He_2(a)$—reaction (7). Helium excimers are produced in three-body collisions of the helium metastable atom with two helium atoms in the ground state—reaction (6).

$$He(2s\,^3S) + H_2O \rightarrow He + H_2O^+(X, A, B) + e^-, \quad (5)$$

$$He(2s\,^3S) + 2He \rightarrow He_2(a) + He, \quad (6)$$

$$He_2(a) + H_2O \rightarrow 2He + H_2O^+(X, A, B) + e^-, \quad (7)$$

$$H_2O^+(A) + e^- \rightarrow OH(A) + H, \quad (8)$$

$$OH(A) \rightarrow OH(X) + h\nu. \quad (9)$$

In neon, similar processes can be expected. Since the production of the metastables is spatially inhomogeneous and has a higher maximum at the cathode and a lower maximum at the anode (see Mangolini *et al* (2004), figure 6 of the reference in particular), two spatially limited light traces of OH emission of different intensities appear between the main intensity maxima. Taking into account the excitation mechanism discussed above, the evolution of the OH emission can be explained by the relative long radiatively lifetime of $H_2O^+(A)$ ions (about 10 μs, see Ricard *et al* (1999)) and the existence of thermalized electrons and $H_2O^+(A)$ ions in front of the anode after the change of polarity. However, these species do not trigger the following discharge pulse. As can be seen clearly in figures 8–10 the development of the cathode directed luminosity wave begins in the middle of the discharge gap and not at the anode.

A very short intensity maximum crossing the gap at the time of 77 μs can be located in some plots in figures 8 and 9. At first this maximum was considered to be a product of the previously mentioned residual current peak. However, since the intensity dependence was always measured during four periods of the voltage signal and the temporal position of this maximum changes in respect of the main maxima,

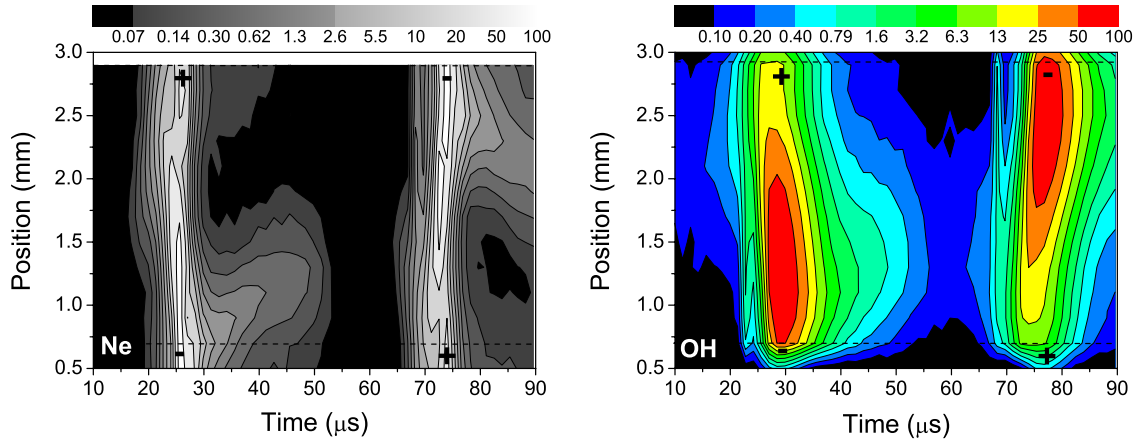

Figure 10. Spatially and temporally resolved intensity distributions of neon SPM diffuse discharge in a 2.2 mm cell. The relative intensity of the neon line at 703.2 nm and the OH system at 309.0 nm are plotted in a logarithmic scale versus the time and the position across the discharge gap. The cathode is located at the bottom first, then at the top. The positions of the electrodes (of the dielectric layers, exactly) are marked out by the dashed lines.

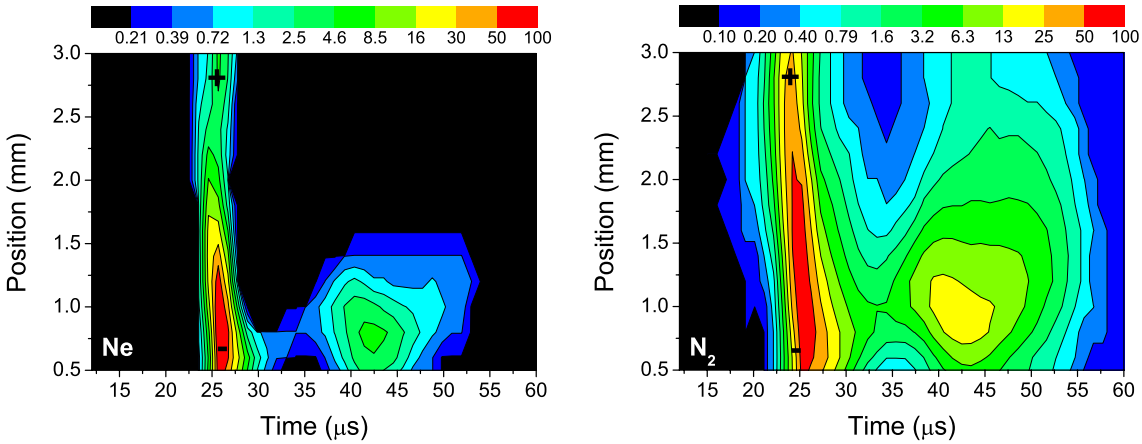

Figure 11. Spatially and temporally resolved intensity distributions of neon DPM diffuse discharge in a 2.2 mm cell. The relative intensity of the neon line at 703.2 nm and the N_2 second positive system at 337.1 nm are plotted in a logarithmic scale versus the time and the position across the discharge gap. The time range covers only the first voltage half period, i.e. only one polarity is shown. The cathode is located at the bottom.

this short maximum could have been produced by a device error.

The diffuse discharge in neon was also studied in the discharge cell with a discharge gap of 2.2 mm. In figure 10 spatially and temporally resolved intensities of the neon line at 703.2 nm and the OH system at 309.0 nm of neon SPM discharge are shown. The temporal resolution was 1.4 μs in this experiment, so the discharge structure is less resolved as in figures 8 and 9. However, the discharge development was investigated to be almost the same as in the 5 mm discharge gap, namely, with a bright cathode light and a less intensive anode region. Solely, the intensity maxima at the cathode were broader. This is probably due to a slight transition from SPM to DPM. A small spatial intensity maximum also appeared near the anode. However, in contrast to the discharge structure in the 5 mm discharge gap (figure 8) no positive column was formed. Thus, it is suggested again that the free electrons cannot be stored in the positive column, and this electron/ion-trapping mechanism fails to explain the mechanism of generating a diffuse DBD in neon. The emission of OH persisted throughout the entire period as in the 5 mm discharge cell. Its spatial distribution clearly determined the discharge gap area.

It is interesting that in argon a filamentary DBD is investigated at the conditions being considered. A comparison of the energetic levels of the metastable states of helium, neon and argon and the ionization energy of N_2 supports the important role of indirect ionization processes, e.g. Penning ionization of N_2 molecules (equations (3) and (4)) as pointed out by different authors (e.g. Massines *et al* (1998), Golubovskii *et al* (2003)). Helium and neon metastables (with excitation energy of 20 eV and 16.6 eV, respectively) and excimers have enough energy to ionize nitrogen directly (ionization energy, 15.6 eV), but argon metastables do not (11.6 eV). Thus, in neon and helium the indirect ionization may produce a preionization level, which is sufficient for an overlapping and a coalescence of electron avalanches, as first proposed by Palmer(1974) and by Levatter and Lin(1980). This avalanche coalescence leads to a suppression of the microdischarges and to the generation of the diffuse regime of the DBD.

The intensity distributions of the neon line at 703.2 nm and the N_2 second positive system at 337.1 nm of neon 2.2 mm DPM diffuse discharge are shown in figure 11. In contrast to the previous figures, figure 11 shows, only, the development within one voltage half period. In this half period the cathode was located at the bottom of the figure. Two intensity maxima with maximum value at the cathode were investigated. These maxima correspond to the two subsequent current peaks of the DPM (compare with figure 4). Both discharge events have a similar structure as the discharge in the SPM, namely, the formation of the cathode light. Between the first and the second discharge the intensity did not decrease to zero. The maximum value of intensity in the second pulse was due to the lower current being generally lower than in the first pulse. However, the ratios of the maximum intensity in the second pulse to the maximum intensity in the first pulse were found to differ for the various emissions. The highest ratio was found for the N_2 second positive system, followed by oxygen emission (not shown here) and neon radiation. These experimental results are in agreement with the spectrally integrated but temporally and radially resolved discharge recordings of Mangolini *et al* (2002) as well as with the results presented by Radu *et al* (2003). The recordings of the former authors revealed that the subsequent discharge pulses are generated due to inhomogeneous charge accumulation on the dielectric in different regions of the discharge volume. This radial discharge development cannot be verified, since our investigation was only one-dimensional.

4. Conclusion

Diffuse DBDs in neon and helium were investigated by electrical measurements and temporally and spatially resolved optical emission spectroscopy. The experiments revealed similar behaviour of the diffuse discharges in neon and helium. Although the breakdown takes place at different electric field strengths, the discharge current development is almost the same for both gases, differing only in the magnitudes of the current density. Furthermore, the measured spatio-temporally resolved intensity evolutions revealed the same structure of the discharges in neon and helium. In agreement with other authors the structure of a transient subnormal glow discharge consisting of a cathode fall, a positive column and an anode fall was observed (glow-like discharge) in helium as well as in neon. The spatial distributions in the 2.2 mm gap were quite similar, but no positive column was observed. Since in argon the filamentary discharge is observed at the same conditions, indirect ionization processes between long-lived excited states (metastables and excimers) and N_2 molecules (Penning ionization) are assumed to be important for the existence of the diffuse DBD in helium and neon. These processes can provide the gas preionization, which is needed for the overlapping of the avalanches leading to the suppression of the microdischarge development and to the generation of the diffuse discharge.

Different discharge regimes were investigated in both gases. The standard regime was named SPM, since a single discharge pulse per voltage half period was registered. However, two or more current peaks per half period (DPM, etc) can be obtained by the voltage increase, or by nitrogen admixture in the range of 100–800 ppm. Our results confirm the findings of various authors, which are, namely, the generation of subsequent discharges due to a re-rise of the gap voltage in combination with a decrease of the breakdown voltage due to the presence of long-lived excited species remaining from the first discharge event.

Acknowledgments

This work was supported by research project MSM0021622411 and grants No 202/05/0777, 202/02/D097 of Czech Science Foundation, Deutsche Forschungsgemeinschaft, SFB 198, 'Kinetics of partially ionized plasmas'. The work of Z Navrátil in Greifswald was supported by Deutscher Akademischer Austausch Dienst (DAAD).

References

Bartnikas R 1968 *Br. J. Appl. Phys.* **1** 659–61
Bojčenko A M, Tarasenko V F, Fomin E A and Jakovlenko S I 1993 *Kvant. Elektron.* **20** 7–30
Brandenburg R, Kozlov K V, Gherardi N, Michel P, Khampan C, Wagner H-E and Massines F 2002 *Hakone VIII Contributed Papers (Tartu, Pühajärve, Estonia)* p 28
Eliasson B and Kogelschatz U 1991 *IEEE Trans. Plasma Sci.* **19** 309–23
Gibalov V I and Pietsch G J 2000 *J. Phys. D: Appl. Phys.* **33** 2618–36
Gherardi N, Gouda G, Gat E, Ricard A and Massines F 2000 *Plasma Sources Sci. Technol.* **9** 340–6
Golubovskii Y B, Maiorov V A, Behnke J and Behnke J F 2003 *J. Phys. D: Appl. Phys.* **36** 39–49
Kim Y and Rudd M E 1994 *Phys. Rev.* A **50** 3954–67
Kozlov K V, Wagner H-E, Brandenburg R and Michel P 2001 *J. Phys. D: Appl. Phys.* **34** 3164–76
Kozlov K V, Brandenburg R, Morozov A M, Wagner H-E and Michel P 2005 *J. Phys. D: Appl. Phys.* **38** 518–29
Levatter J and Lin S-C 1980 *J. Appl. Phys.* **51** 210–22
Lissovski A and Treshchalov A 2003 *ICPIG: Proc. 26th Int. Conf. on Phenomena of Ionized Gases (Greifswald)* p 247
Mangolini L, Orlov K, Kortshagen U, Heberlein J and Kogelschatz U 2002 *Appl. Phys. Lett.* **80** 1722–4
Mangolini L, Anderson C, Heberlein J and Kortshagen U 2004 *J. Phys. D: Appl. Phys.* **37** 1021–30
Massines F, Rabehi A, Décomps P, Ben Gadri R, Séguer P and Mayoux C 1998 *J. Appl. Phys.* **83** 2950–7
Meneses G D, Clark R E H, Abdallah J Jr and Csanak G 2002 *J. Phys. B: At. Mol. Opt. Phys.* **35** 3119–36
Müller S and Zahn R-J 1996 *Contrib. Plasma Phys.* **36** 697–709
Palmer A J 1974 *Appl. Phys. Lett.* **25** 138–40
Radu I, Bartnikas R and Wertheimer M R 2003 *IEEE Trans. Plasma Sci.* **31** 1363–78
Radu I, Bartnikas R and Wertheimer M R 2004 *J. Phys. D: Appl. Phys.* **37** 449–62
Raizer Y P 1991 *Gas Discharge Physics* (Berlin: Springer) p 169
Ricard A, Décomps P and Massines F 1999 *Surf. Coat. Technol.* **112** 1–4
Rutscher A and Pfau S 1976 *Physica* C **81** 395–402
Trunec D, Brablec A and Buchta J 2001 *J. Phys. D: Appl. Phys.* **34** 1697–9
Wetzel R C, Baiocchi F A, Hayes T R and Freund R S 1987 *Phys. Rev.* A **35** 559–77